ELSEVIER

International Journal of Applied Earth Observation and Geoinformation 7 (2005) 29–48

INTERNATIONAL JOURNAL OF APPLIED EARTH OBSERVATION AND GEOINFORMATION

www.elsevier.com/locate/jag

Assessing land cover change resulting from large surface mining development

Rasim Latifovic[a,*], Kostas Fytas[b], Jing Chen[c], Jacek Paraszczak[b]

[a]*Natural Resources Canada, Earth Sciences Sector, Canada Centre for Remote Sensing, 588 Booth Street, Ottawa, Ont., Canada K1A 0Y7*

[b]*Département de génie des mines de la métallurgie et dés materiaux, Université Laval Québec, Canada*

[c]*Department of Geography, University Toronto, Canada*

Received 22 July 2004; accepted 2 November 2004

Abstract

A remote sensing based land cover change assessment methodology is presented and applied to a case study of the Oil Sands Mining Development in Athabasca, Alta., Canada. The primary impact was assessed using an information extraction method applied to two LANDSAT scenes. The analysis based on derived land cover maps shows a decrease of natural vegetation in the study area (715,094 ha) for 2001 approximately −8.64% relative to 1992. Secondary assessment based on a key resources indicator (KRI), calculated using normalized difference vegetation index (NDVI measurements acquired by NOAA–AVHRR satellites), air temperature and global radiation was performed for a time period from 1990 to 2002. KRI trend analysis indicates a slightly decreasing trend in vegetation greenness in close proximity to the mining development. A good agreement between the time series of inter-annual variations in NDVI and air temperature is observed increasing the confidence of NDVI as an indicator for assessing vegetation productivity and its sensitivity to changes in local conditions.

Keywords: Remote sensing; Land cover; Environmental impact assessment; Surface mining

1. Introduction

Quantification of the effects that mining activities have on ecosystems is a major issue in sustainable development and resources management. The conflict between mining activities and environmental protection has intensified over recent years, emphasizing the need for improved information on the dynamics of impacts at regional and local scales. Assessing cumulative environmental impacts is an important aspect of sustainable management and involves balancing benefits from resource exploitation against environmental degradation. The success in defining an appropriate balance directly depends on our ability to quantitatively predict and assess impacts on the environment caused by industrial developments.

* Corresponding author. Tel.: +1 613 947 1816; fax: +1 613 947 1383.

E-mail address: rasim.latifovic@ccrs.nrcan.gc.ca (R. Latifovic).

0303-2434/$ – see front matter.
doi:10.1016/j.jag.2004.11.003

The difficulties in addressing the effects of mining development are accentuated by the fact that the effects of many types of disturbance are similar, and that responses of plants to several stressors do not allow for identification of the specific source. Stress has many causes and collateral effects such as insects and disease that further damage plants in their already weakened state. Sorting out causes and effects is a challenging task and is critical for assessing and mitigating the impact mining might have on the surrounding environment.

A successful monitoring approach for evaluating surface processes and their dynamics at a regional scale requires observations with frequent temporal coverage over a long period of time in order to differentiate natural changes from those associated with human activities. However, long-term field observations in remote areas that have recently become suitable for mining development are typically not available. Systematic long-term measurements of vegetation properties in such remote areas usually cannot be economically justified prior to mining development. In most cases, remote sensing is the only alternative to field collected observations when a historical record is needed for studying the long-term vegetation cycles. So far, the only available source of long-term terrestrial observations is data collected by several generations of NOAA AVHRR and LANDSAT satellites. The AVHRR (advanced very high resolution radiometer) onboard a series of NOAA satellites have provided daily measurements since 1979 with a coarse spatial resolution of 1.1 km. Despite numerous limitations, the AVHRR historical time series is considered as a primary data set for terrestrial monitoring at regional or global scales. LANDSAT MSS, TM and ETM+, with medium spatial resolutions (30–80 m pixel size) have provided measurements since 1972 at a temporal resolution of 16–18 days.

In addition to being the only available data source in many areas, remote sensing has the added advantage of acquiring data with sufficient area coverage and temporal frequency for studying and monitoring primary impacts caused by surface mining at low cost. It can also be used for studying atmospheric emissions and water pollution indirectly by monitoring green vegetation, an indicator of ecosystem health and conditions. A number of published papers (Ress and Williams, 1997; Schmidt and Glaesser, 1998; Prakash and Gupta, 1998; Wright and Stow, 1999; Olthof and King, 2000) suggest usefulness of such techniques for detecting contamination, determining success in reclaiming open cast mined areas and for providing other relevant spatial data for assessing mining impact on the environment. Since the 1970s analog aerial photographs have been used for mapping spatial changes in mined areas (Anderson, 1977; Schneider, 1984) and for monitoring reclamation success (Barr, 1981; Mamula, 1978).

Since the 1980s vegetation phenology has been studied over broad scales using AVHRR time series (Ducemin et al., 1999; Justice et al., 1985; Townshend et al., 1991). Some of the work focused on producing characteristic phenologies and monitoring surface dynamics for evaluating intra-annual deviations from baseline conditions, while other work was directed at mapping land cover distribution using various methods (Tucker et al., 1985; Malingreau, 1986; Malingreau et al., 1989; Loveland et al., 1991; Loveland and Belward, 1997; Townshend, 1994; DeFries et al., 1995; Cihlar et al., 1996; Nenami and Running, 1997; Gopal et al., 1994).

The numerous studies of remote sensing for environmental monitoring indicate that remote sensing observations are becoming increasingly important tools for studying different aspects of ecosystems at local, regional and global scales. It is also evident that satellite based remote sensing is widely accepted and utilized by different disciplines, often related to environmental condition, ecosystem dynamics e.g. atmosphere, biosphere and hydrosphere exchanges. However, the lack of studies related to environmental impacts of mining and remote sensing indicates under-utilization in this sector. Therefore, the objective of this study was to provide an initial assessment approach based on remote sensing data and evaluate the use of such data in investigating trends in vegetation productivity in order to assess the rate of abrupt and transitional land cover changes in the Athabaska Oil Sands region.

2. Methods

2.1. Study area

The study area is located north of Fort McMurray, Alta., in the Athabasca Oil Sands region (Fig. 1). The

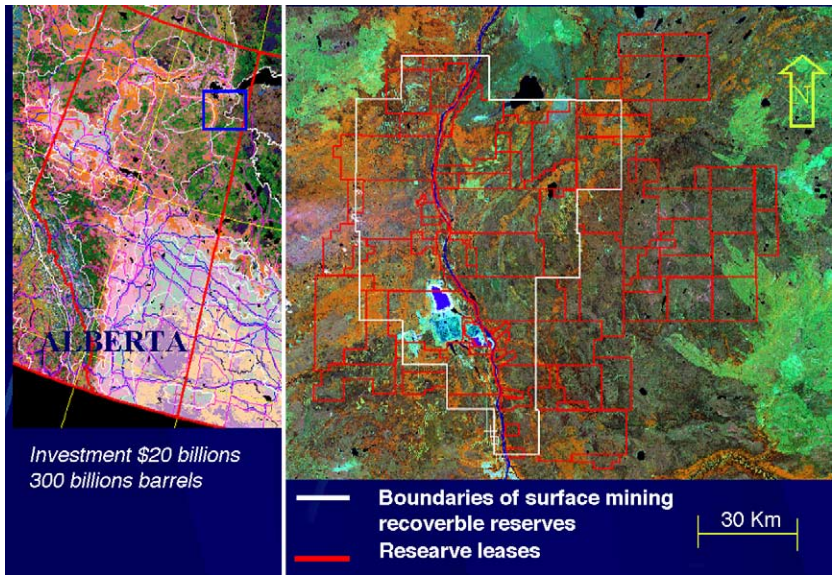

Fig. 1. A general view of the Athabasca Oil Sends study area located in northeast Alberta. The white boundary outlines area of recoverable oil sands reserves. The red boundaries outline exploration leases.

region is in the Boreal Plains ecozone, and includes fractions of three ecoregions according to the Canadian Ecological Land Classification System (1995): Wabasca Lowland (ecoregion number 142) in the southwest, Slave River Lowland (ecoregion number 136) in the north and Boreal Uplands (ecoregion number 147) in the west. Cool summers and long cold winters characterize the subhumid mid-boreal ecoclimate type with mean annual temperature of 0.5 °C and mean annual precipitation ranging from 350 to 500 mm. Dominant vegetation types are medium to closed canopy stands of aspen (*Populus tremuloides*) and balsam poplar (*Populus balsamifera*) with white spruce (*Picea glauca*), black spruce (*Picea mariana*) and balsam fir (*Abies balsamea*). Cold poorly drained fens and bogs are covered with tamarack (*Larix laricina*) and black spruce. Organic soil is dominant covering 50% of the region. Land uses include forestry, water oriented recreation, wildlife hunting and trapping, and oil and gas exploration.

In addition to mining and processing of oil sands, other industrial activities are present in the region that also can contribute to stress on the surrounding environment, such as timber harvesting, urban growth in Fort McMurray and Fort McKay, and new linear disturbances such as exploration seismic lines, roads and pipelines.

2.2. Spatial and temporal approach

An important goal in monitoring vegetation condition is to provide data for predicting incremental effects resulting from the combined influences of various stressors. Long-term impacts on the environment can be caused by, not only individual activities, but also by the combined effects of successive activities. These incremental effects may be significant even though the effects of each action, when independently assessed, are considered insignificant. Large-scale surface mining and processing operations at the Athabasca Oil Sands (AOS) region is the case where extensive development of long duration covering a large area may have significant cumulative effects on the regional ecosystem. In addition to a large surface disturbance, potential mining impacts on vegetation in this region can also arise from acidification of soils, acute leaf exposure to SO_2, metal deposition, excess nitrogen fertilization, and deposition and uptake of ground-level ozone and organic compounds emitted by the oil sand processing

facilities. As with acid deposition, response to stress can be either acute or chronic, affecting the viability of plants primarily by interfering with photosynthesis (Krupa and Kickert, 1989). The combined effects of soil acidification, exposure of vegetation to SO_2, NO_x and O_3, metal deposition, and nitrogen deposition are not sufficiently understood to allow their effects to be accurately predicted. In cases where assessment and prediction of individual cause–effects is difficult, focusing on key resources indicator (KRIs) can be an effective means of assessment. The KRIs are used in impact assessment studies because environmental systems include a very large number of complex interconnected elements, with each element contributing to the functioning of an ecosystem as a whole. Such an indicator is selected for the entire system to represent the range of ecological activities that is being studied.

To facilitate the analysis in this study, the effects on vegetation are separated into primary and secondary impacts. Primary impacts are considered as all surface disturbances resulting from exploration, mining development, urban development and logging. Secondary impacts are considered as all changes in vegetation productivity resulting from pollutant uptake and deposition, changes in available water capacity or any other changes in growing conditions caused by development.

The primary impact was identified by mapping baseline and current land cover distributions using two LANDSAT scenes. Post-classification change detection methods were then employed to assess primary impacts.

The secondary impact assessment is based on a KRI approach where a selected indicator is related to vegetation net primary productivity (NPP). The KRI is computed from AVHRR surface reflectance time series (1990–2002) as the integrated normalized difference vegetation index (NDVI) over the peak of growing season and its relation to the fraction of photosynthetically active radiation (FPAR), average temperature and incoming solar radiation. NDVI is selected as a key parameter because it has been associated with morphological or physiological indicators of plant growth and vigor, such as biomass, leaf area index (LAI), and FPAR. Information derived from NDVI can be related to long-term meteorological events, plant species distribution or human induced changes in terrestrial vegetation.

A theoretical comparison of NDVI with photosynthesis and transpiration models suggest that for vegetation experiencing optimal temperature and water availability, NDVI might be directly related to canopy CO_2, H_2O exchange and conductance. The relation of NPP to NDVI is based on the premise that plant production is related to both the absorbed and reflected radiation by green vegetation. An in-depth technical description of how reflected light energy such as that received from the AVHRR sensors can be used as surrogates for estimating NPP as well as other biophysical properties is available elsewhere (Sallers, 1985, 1987; Sallers et al., 1992; Tucker and Sallers, 1986; Running and Ramakrishna, 1988).

The use of the NPP–NDVI relation for assessing secondary impacts is based on the following hypothesis: a deviation in the KRI multiyear trend estimated from measured NDVI and the KRI trend estimated by a simulation model driven only by environmental condition (such as temperature, global radiation, etc.) indicates an influence of other factors not accounted by the model e.g. a significant presence of air pollutants such as SO_2, NO_x and O_3, a change in water condition or other stressors. The hypothesis assumes that following two requirements are met:

1. A seasonal NDVI trend can approximately represent the seasonal rates of photosynthesis and transpiration of natural forest cover, thus annual integration of NDVI correlates with annual NPP.
2. Other long-term factors that influence NPP such as soil type, terrain aspect and slope, and availability of nutrition are assumed constant i.e. they do not influence the inter-annual comparison.

Two types of models are typically used for mapping NPP at regional scales namely process and production efficiency (or ‘epsilon’) models (Cramer et al., 1999). Process models derive NPP by simulating a series of plant physiological processes, while production efficiency models are based on light use efficiency. The latter models combine simple equations for estimating NPP by relating NPP to absorbed photosynthetically active radiation under non-stressed conditions. Although each method for determining NPP is slightly different, the use of various summations of NDVI over a growing season is common to all of them (Markon

and Peterson, 2002). Goward et al. (1985) found a strong relationship between NDVI integrated over the growing season and NPP for 12 biomes in North America. Similar results confirming the relation between NPP and NDVI have been reported elsewhere (Box et al., 1989; Benedetti and Rossini, 1993; Jang et al., 1996).

The KRI used in this study for assessing secondary impacts is computed based on the well-known GPP approach of Kumar and Monteith (1981):

$$\begin{aligned} \mathrm{GPP} &= p(T) \times \mathrm{CO}_{2_{\mathrm{fert}}} \times \varepsilon \times f_{\mathrm{PAR}} \times c \times s(S_{\mathrm{gr}}), \\ \mathrm{NPP} &= \mathrm{GPP}(1 - A) \end{aligned} \tag{1}$$

where GPP is the gross primary production representing the gross uptake of carbon by photosynthesis; NPP the net primary production; c the climate efficiency; $p(T)$ the normalized temperature dependency factor; $\mathrm{CO}_{2_{\mathrm{fert}}}$ the normalized CO_2 fertilization factor; f_{PAR} the fraction of absorbed PAR; ε the photosynthetic efficiency; s the normalized global radiation dependency factor; S_{gr} the incoming solar radiation; A the autotrophic respiration.

Asfsuming a linear relation between NDVI and f_{PAR} (Sallers, 1985, 1987) and holding other long-term factors constant ($\mathrm{CO}_{2_{\mathrm{fert}}}$, ε and c) during the comparison period, an NPP based indicator that roughly accounts for environmental condition is computed as:

$$\mathrm{KRI} = p(T) \times s(S_{\mathrm{gr}}) \times \mathrm{NDVI} \tag{2}$$

where dependence of stomatal resistance on environmental condition to temperature and global radiation is described by the Jarvis–Stewart approach (Jarvis, 1976; Stewart, 1988):

$$p(T) = \left(\frac{t_{\mathrm{a}} - T_1}{T_2 - T_1}\right)\left(\frac{T_3 - t_{\mathrm{a}}}{T_3 - T_2}\right)^{T_3 - T_2 / T_2 - T_1} \tag{3}$$

where t_{a} is the actual temperature; T_1 the minimum temperature (=0 °C); T_2 the optimum temperature (=20 °C); T_3 the maximal temperature (=30 °C).

Incoming solar radiation calculated as:

$$s(S_{\mathrm{gr}}) = \frac{S_t}{S_1}\left(\frac{S_1 + S_2}{S_t - S_2}\right) \tag{4}$$

S_t is the actual global radiation [W m^{-2}]; S_1 = 1000 W m^{-2}; S_2 = 125 W m^{-2}.

KRI trend analysis was focused on answering two basic questions: what are the trends and variations in KRI over time and space? The spatial trend in KRI was examined in relation to the proximity of the surface mining operation in order to assess the extent of the impact zone. An additive parameter field can represent the KRI's spatial and temporal variations. This assumes that the variability in KRI or NDVI can be decomposed into three independent types of variation:

- a deterministic or trend component;
- seasonality or cyclical variations;
- stochastic or irregular variations.

Regular variations in a KRI time series may result from a tendency to follow some cyclical pattern through time, for example seasonal variation in vegetation growth conditions. The seasonal and cyclical variations are most often caused by phenological cycles that are controlled by environmental parameters such as air temperature and global radiation. Random or irregular variations can be caused by human activities, such as logging, mining and other industrial developments, or caused by natural disturbances such as forest fire, flood, or severe weather conditions.

2.3. Experimental design

In order to relate surface disturbance and trends in vegetation growth to the proximity of surface mining operations, the study area was spatially delineated into three separate impact zones using potential acid input (PAI) prediction. PAI is the preferred method for evaluating overall effects of acid forming chemicals on the environment since it accounts for the acidifying effect of sulfur and nitrogen species, as well as the neutralizing effect of available base cations. The PAI prediction used in this study is adopted from the Suncor In Situ Oil Sands application. Annual concentration and deposition were predicted using CALPUFF a multi-layer, multi species non-steady-state puff dispersion model which can simulate the effects of time and space varying methodological condition on pollutant transport, transformation and removal (EPA, 1995).

Three impact zones were defined using isopleths maps representing annual PAI and generic critical load values taken from the Clean Air Strategic Alliance (CASA) (Target Loading Subgroup, 1996): low deposition (0.25 keq/ha/year), medium deposition

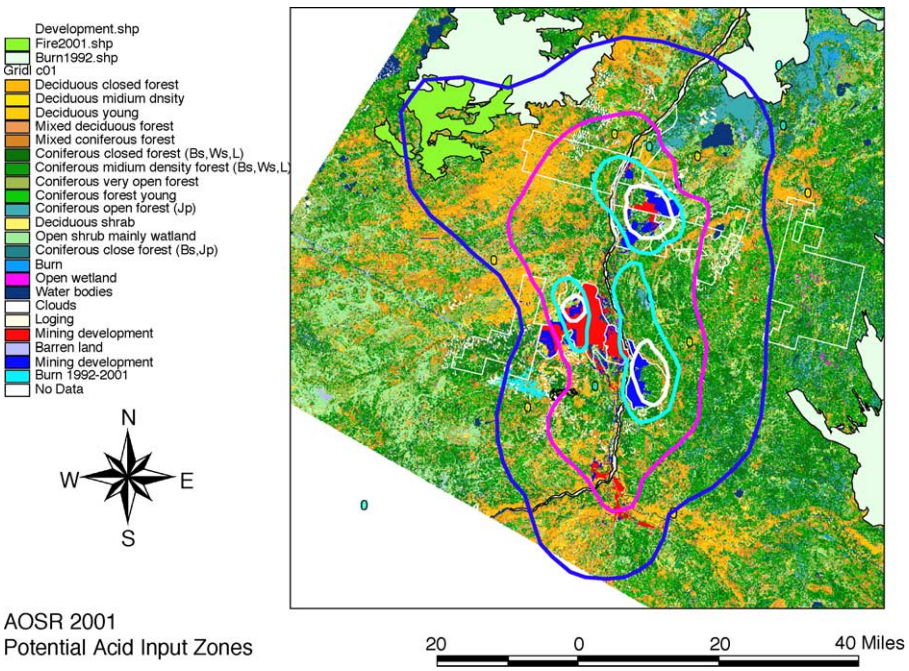

Fig. 2. Spatial distribution of annual potential acid input predicted by CALPUFF model run (adopted from in situ Oil Sands Application Firebeg Project).

(0.5 keq/ha/year) and high deposition (1.00 keq/ha/year) (Fig. 2). In the following text these areas are referred as Zone-PAI 0.25, Zone-PAI 0.50 and Zone-PAI 0.75.

Direct surface disturbances are assessed for each impact zone by comparing the baseline 1992 versus the current 2001 conditions as defined by land cover maps.

Secondary impacts are ascertained using the KRI trend analysis in the three rings surrounding the surface mining development. The spatial extent of the rings are defined by PAI ranges with Ring-PAI 0.25 the area covered by $0.25 > \text{PAI} < 0.50$ keq/ha/year, Ring-PAI 0.50 is the area in which $0.50 > \text{PAI} < 0.75$ keq/ha/year and Ring-PAI 0.75 is the area in which PAI > 0.75 keq/ha/year.

A seasonal-trend decomposition procedure based on Loess smoothing (STL) with a moving time window of 3 years and tricub weight function was used for decomposition of the KRI time series into seasonal and random trend components. STL has simple design that consists of a sequence of applications of Loess smoother (Cleveland et al., 1990).

3. Data and data processing

3.1. Medium resolution satellite data

3.1.1. Scene selection and study area boundary

Remote sensing based land cover mapping was conducted over the AOS region within the extents of a single LANDSAT scene. The three images used in this study are—(1) LANDSAT 5 TM path: 43, row: 20 acquired on 11 June 1992; (2) LANDSAT 7 ETM+ path: 43, row: 20 acquired on 17 August 1999; (3) LANDSAT7 ETM+ path: 42, row 20 acquired on 23 August 2001. The selected images span a 9-year period during the most intensive mining activity.

3.1.2. Scene geometric rectification

Geometric rectification of the selected images was performed using 20 geographically dispersed ground control points (GCPs) with a first order polynomial and nearest neighbour resampling. An average RMS error below 1.0 pixel was targeted as an acceptable rectification goal. For the 1992 LANDSAT scene an RMS error of 0.65 pixel was achieved. In order to

correctly co-register the 1999 and 2001 scenes with the geo-rectified 1992 scene, pixels were identified in each scene corresponding to geo-referenced pixels in the 1992 scene. Rectification of the 1999 and 2001 scenes was performed using these pixels as GCPs. The RMS errors for each geo-rectification were 0.35 pixels and 0.38 for the 1999 and 2001 scene, respectively.

3.1.3. Scene radiometric normalization

Variation in solar illumination condition, phenology and detector performance results in differences in radiance values unrelated to the reflectance of the land surface. Radiometric normalization was performed using the approach given by Du et al. (2001). The process consist of the following steps: (1) selection of pixels pairs in overlap area; (2) principal component analysis for the selection of characteristic pixels; (3) calculation of gain and offset; (4) radiometric normalization.

3.1.4. Land cover classification

Selected scenes were classified into 15 land cover classes following the method described in Cihlar et al. (1998) and Latifovic et al. (1999). The images were enhanced using a linear stretch as in Beaubien (1986) to equalize the dynamic range of each spectral band.

Table 1
Description and hierarchical structure of landscape classes

Landscape class	Description	Label	Clusters
Vegetated natural origin			
Deciduous forest			
Deciduous forest	Deciduous trees (aspen, birch, balsam poplar) greater than 60% canopy cover	1	1, 2, 3
Mixedwood forest			
Broadleaf mixed	Deciduous and conifer trees aspen–pine, aspen–white spruce or balsam poplar–white spruce where deciduous fraction is more than 60%. Canopy cover more than 60%	4	4
Coniferous mixed	Coniferous and deciduous trees where coniferous fraction is more than 60%. Canopy cover more than 60%	5	5
Coniferous forest			
Black spruce forest	Coniferous trees mainly black Spruce with fraction of white spruce and pine. Mosses and shrub dominate in understory. Canopy cover greater than 60%	6	6, 7
Black spruce young forest	Generally young forest after old perturbation	9	9
Pine forest	Coniferous trees manly jack pine with lichen and some shrub in understory. Canopy cover less than 60%	10	10
Pine–black spruce forest	Coniferous trees co-dominant black spruce, jack pine. Mosses forbs and shrub in understory. Canopy cover more than 60%	13	
Non-forest			
Treed	Sparse coniferous tree less than 25% canopy covers. Commonly located on poor sites associated with wetland. This class usually includes a proportion of broadleaf vegetation mostly shrub	8	8, 12
Deciduous shrub	Dominated by shrubland or grassland	11	
Burn	Burn are usually characterized by sparse vegetation cover varying with the age and intensity of a burn	14	14, 22
Open wetland	Open fen, marsh, or swamp	15	
Non-vegetation			
Barren land	Bare soil, rock space herbaceous and grass	20	
Water		16	
Anthropogenic origin			
Disturbance	Forestry cutblock, forestry cutblock regrowth	18	
Industrial development	Surface mining, build-up, roads, and exploration lines	19	19, 21
No data	Clouds, shadows	17	

All pixels in the full-resolution enhanced image were classified into 150 spectral clusters using a K-means classifier. Further cluster agglomeration was performed based on cluster spectral similarity and spatial proximity. The procedure employs basic statistical parameters that determine between cluster spatial proximity and within cluster spectral space data distributions. It uses the arithmetic mean of clusters to compute the Euclidean distance between cluster pairs and the standard deviation to represent clusters' ellipsoid major axis and orientation relative to other clusters. Spectral clusters are first sorted according to decreasing size and then examined for the most similar cluster pairs, starting with the smallest clusters. The spatial criterion is based on the property that many spectral clusters represent gradients within cover types and for these clusters there frequently exists a strong relationship between their spatial and spectral characteristics. The agglomeration procedure utilizes this relationship as a weighting function in computing cluster similarity. More detail on the agglomeration procedure is provided in Latifovic et al. (1999). The agglomeration yielded 55 significantly different spectral clusters further grouped into 15 land cover classes and labeled according to the legend provided in Table 1. Post-classification refinement included corrections in delineating forest cutblocks, urban and mining development leading to the final land cover maps presented in Fig. 3

Two land cover maps were compared to each other to assess map consistency and then to reference data to assess accuracy. The reference data were project footprints obtained from Environmental Impact Assessment Studies of Millennium, Muskeg River and Forth Hills Oil Sands Projects. Other reference data used for the assessment included segments of AlPac Alberta vegetation inventory based on interpretation of 1:20,000 scale aerial photographs from 1991 and series of reports on the Terrestrial Environmental Effect Monitoring (TEEM) Program of the Wood Buffalo Environmental Association (WBEA).

Map consistency assessment was performed on a pixel basis over the area that did not undergo change from direct impacts by comparison of pixel label agreement. The assumption was that if both classifications map the same temporally stable pixel with the same label, confidence in mapping accuracy increases.

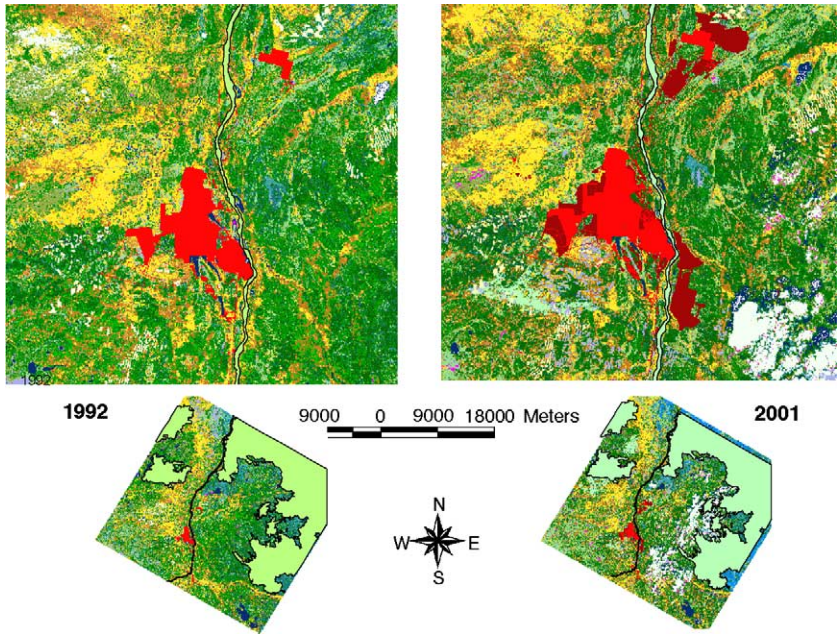

Fig. 3. Athabasca Oil Sands region landscape classifications baseline condition in 1992 and current condition in 2001, derived from LANDSAT TM/ETM+ satellite data.

For example, 90% of all pixels mapped as broadleaf forest in the 1992 land cover map were also classified with the same label in the 2001 land cover map. Overall average agreement of all classes weighted by class extent was 87%. Higher consistency was achieved in mapping forest classes (92%) than in mapping non-forest classes 75%. An analysis of pixels in disagreement showed confusion between spectrally similar or transitional land cover types such as broadleaf forest and broadleaf shrub, treed and wetland or different coniferous sub-classes. Spectrally distinguishable classes, for example, disturb area and forest classes were separated well with an average accuracy of 94%.

3.2. Coarse resolution satellite data

A post-seasonal systematic correction procedure, described in Cihlar et al. (2004), was applied to the AVHRR time series. It included atmospheric correction, BRDF normalization, screening and temporal interpolation for replacement of measurements affected by cloud and aerosol contamination. Significant improvements have been incorporated into the correction procedure based on recently published algorithms for atmospheric correction (Trishchenko et al., 2002), bi-directional reflectance normalization (Latifovic et al., 2001), cloud screening and temporal interpolation (Cihlar et al., 1999) and radiometric calibration (Fedosejevs et al., 2000). The AVHRR time series were corrected using AVHRR Manager; a software package developed for this purpose.

The initial AVHRR data set contains 10-day image composites for the 1990–2002 growing seasons acquired by the NOAA 11, 14 and 16 satellites. Each growing season is represented by twenty 10-day composites between 11 April and 31 October. In addition to AVHRR, SPOT 4 VEGETATION (VGT) composite data from 11 April to 31 October, 1998–2002 were also used in this study as a control data set.

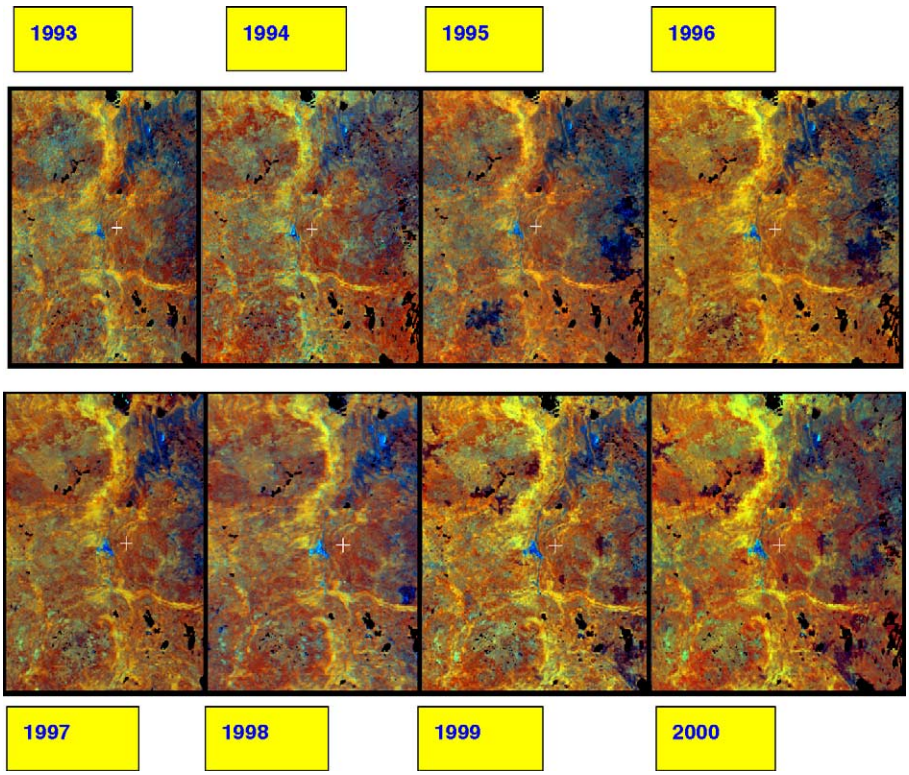

Fig. 4. The three band image R: NDVI, G: NIR, B: red illustrates an example of corrected AVHRR 10-days composites over the Athabasca Oil Sands region.

Differences between the spectral respond functions of NOAA14 and NOAA16 sensors, elaborated in Trishchenko et al. (2001), cause a significant disparity in NDVI measurements. Thus, NDVI measurements were normalized using VGT data, which was acquired during the NOAA14 (1998–2000) and NOAA16 (2001, 2002) operational window. An example of corrected and normalized AVHRR 10-day composites are illustrated in Fig. 4.

3.3. Meteorological data

The meteorological data set over the AOS region was extracted from the DS472.0-TDL US and Canada surface hourly observations generated by the Data Support Section (DSS) of the National Center of Atmospheric Research (NCAR) in Colorado, US. The complete data set includes measurements of about 1000 meteorological stations across the US and Canada for the period from 1976 to 2000. In this study, measurements of air temperature at the five closest stations (Table 2) to the AOS region were extracted and analyzed. In addition to NCAR, the metrological data collected by Air Quality Monitoring Stations of the Wood Buffalo Environmental Association (WBEA) for the period from 1998 to 2002 were also included and analyzed.

4. Results and discussion

4.1. Cumulative and project specific impacts on land cover distribution

Cumulative and project specific impacts on the landscape are quantified using a post-classification change detection method. This method assumes that reference and compared images are classified to a common legend and that the classification method utilized for landscape mapping provides a high accuracy for both images. Landscape changes are simply detected as differences between pixels' labels.

Table 2
Geographical locations of meteorological stations

	Station ID	Longitude [dd]	Latitude [dd]
Forth McMurray	YMM	−111.22	56.65
High Level	YOJ	−117.17	58.62
Peace River	YPE	−117.43	56.23
Forth Chipewyan	YPY	−111.12	58.77
Slave Lake	YZH	−114.78	55.30

Changes in the landscape distribution in the AOS region for the period 1992–2001 were quantified as the difference between classified images from 1992 and 2001. The assessed areas spatially coincide with the impact zones. The Zone-PAI 0.25 that incorporates the other two zones encompasses 715,094 ha. In 1992 Zone-PAI 0.25 was dominated by native forest vegetation, with natural forest landscape classes occupying 75.62% of the area (Fig. 5, Table 3). Coniferous forest covered approximately half (48%), deciduous forest 13% and mixedwood forest covered 15% of the area. The remaining 24% of the area consisted of broadleaf shrub, non-forested and open wetland, water bodies, developed land (including active surface mining, roads and built-up), barren land and forest of anthropogenic origin (cutblocks). Two anthropogenic classes together covered 3.81% of the area, or 27,231 ha.

In 2001 Zone-PAI > 0.25 exhibited a similar landscape class distribution as in 1992 but with a slight decrease in the area covered by natural vegetation. From 1992 to 2001, forest-covered area had decreased from 75.62 to 73.78%, while the area covered by natural non-forest vegetation decreased from 20.57 to 19.10%. The areas occupied by the two anthropogenic classes have increased from 3.81 to 7.12% during the same period (Table 3). Mining area increased from 20,393 to 38,008 ha and forest cutblocks from 6838 to 12,920 ha.

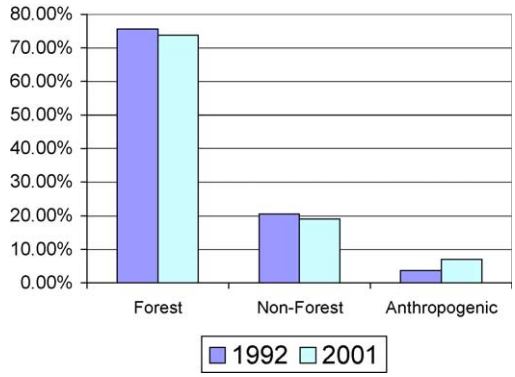

Fig. 5. Area occupied by forest, non-forest and anthropogenic landscape classes in Athabasca Oil Sands Region in 1992 and 2001.

Table 3
Ahabasca Oil Sands Region landscape fraction and class distribution for baseline 1992 and current 2001 conditions

Land cover type [ha]	1992			2001		
	PAI > 0.25	PAI > 0.50	PAI > 0.75	PAI > 0.25	PAI > 0.50	PAI > 0.75
Broadleaf	95417	39589	12639	104410	32819	6934
Coniferous mixed	35860	14521	5325	39199	15333	6122
Broadleaf mixed	69635	27135	9475	75212	29570	9769
Coniferous HD	238475	95031	47577	212751	79730	38805
Coniferous young	58551	23193	8467	62835	26679	11383
Coniferous JP	18312	3066	1705	16912	2154	939
Coniferous JP + BS	24529	6916	4156	16295	5158	2564
Coniferous LD	84855	29111	14444	104587	38225	17752
Broadleaf shrub	24595	9609	4235	9961	2857	758
Burn	11171	481	220	3447	40	10
Open wetland	1193	357	171	231	77	47
Water	16571	8062	5034	12507	5892	3882
Barren land	8698	2495	1225	5819	2887	1294
Logging	6838	2645	431	12920	5097	709
Mining	20393	17482	14423	38008	33177	28559
Sum	715094	279693	129526	715094	279693	129526
Forest	540779	209451	89343	527613	191442	76516
Non-forest	147083	50115	25328	136552	49977	23742
Anthropogenic	27231	20127	14854	50929	38274	29268
Forest (%)	75.62	74.89	68.98	73.78	68.45	59.07
Non-forest (%)	20.57	17.92	19.55	19.10	17.87	18.33
Anthropogenic (%)	3.81	7.20	11.47	7.12	13.68	22.60

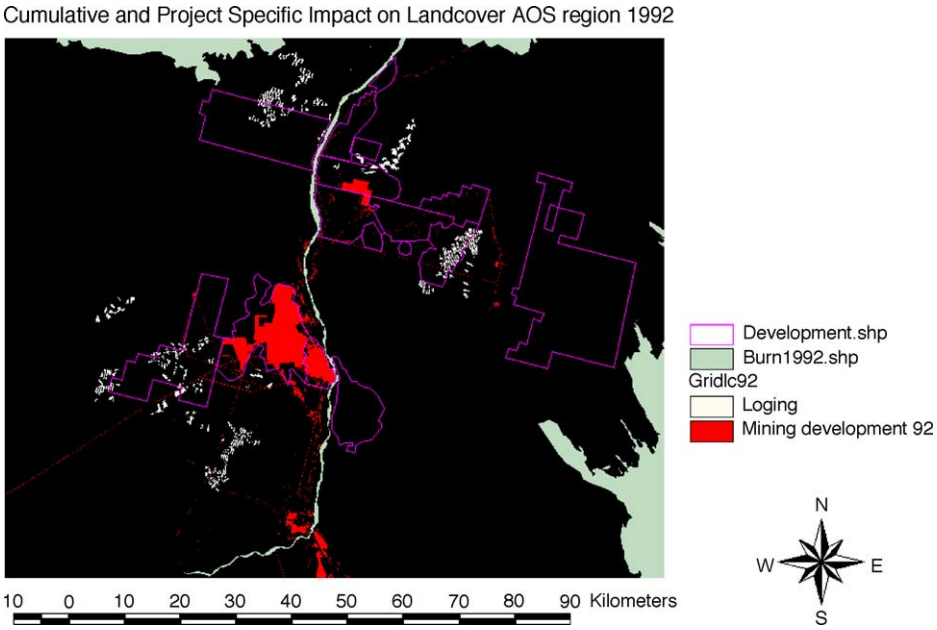

Fig. 6. Anthropogenic landscape classes spatial distribution in Athabasca Oil Sands region in 1992.

The spatial distribution of the areas that have undergone change are illustrated in Figs. 6 and 7. These figures show an increase in the disturbed area resulting mainly from new developments north and west of the mining development that existed in 1992. An increase in logging activities is also evident, in most cases spatially adjacent to the existing mine site or planned mining developments. However, the amount of logging activity associated with the existence of mining development cannot be evaluated from the data used in this assessment.

An analysis of the landscape distribution as a function of proximity to the mining development offers additional insights into the class area changes. Table 3 specifies the landscape class distributions in three surrounding rings at different distances from the mine site. Between 1992 and 2001 the landscape distributions in the Ring-PAI 0.25, the farthest from the mine sites, are more similar than in the Ring-PAI 0.75, which is the closest to the mining development. This difference can be explained mainly by direct impacts due to new surface mining developments in the Ring-PAI 0.75 i.e. the Albian Muskeg River, Millennium, Steepbank and the Aurora North mines, and secondly by logging activities. Areas occupied by the broadleaf and coniferous high-density forest classes have decreased in 2001 by 4 and 7%, respectively, compared to area fractions occupied by the same classes in 1992.

Fig. 8 shows the changes in forest, water bodies, mining and logging classes relative to 1992 in each ring. For example the area affected by mining in 2001 has doubled in size since 1992. The graph (b) in Fig. 8 merits special attention since it exhibits (~25%) decrease in the area of open water bodies. Significant decreases are evident in the vicinity of the Mildred and north mines, suggesting impacts on local hydrology due to these long-term mining operations. Examination of LANDSAT scenes from 1999 and 2002 as well as an ASTER scene from 2000 (15 m spatial resolution) confirmed shrinking of water bodies in the area south west of the Mildred and north mines. These findings need to be confirmed by more detailed analysis of in situ hydrological measurements because the influence on wetland and surrounding vegetation due to a lowering water table could cause significant impacts. The other three graphs in Fig. 8 show an overall decrease in natural forest in 2001, an increase in area affected by logging activities for all three rings and a significant increase in disturbed area by surface mining.

Regardless of relatively high mapping consistency we consider the direct impact presented here as

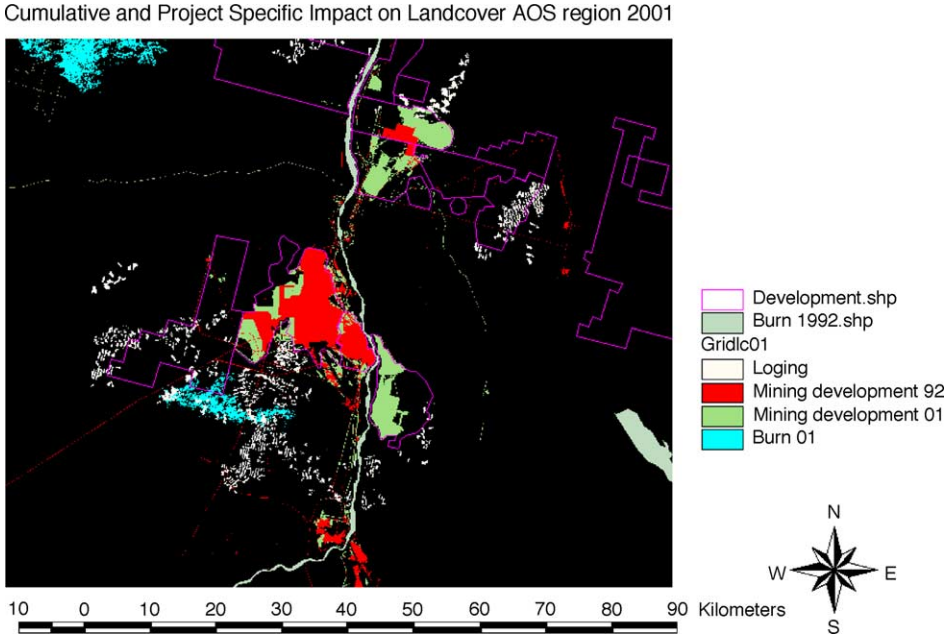

Fig. 7. Anthropogenic landscape classes spatial distribution in Athabasca Oil Sands region in 2001.

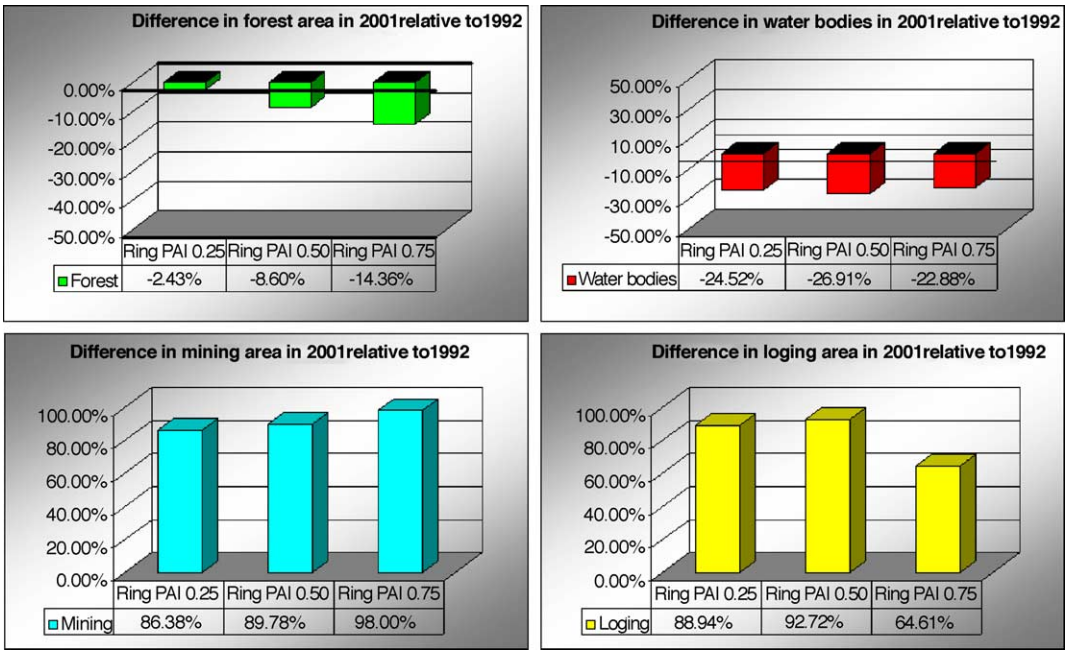

Fig. 8. Difference in class area relative to 1992: (a) mining; (b) water bodies; (c) logging; (d) forested.

approximate due to the limited capability of medium resolution data to depict small changes less than a pixel size (30 m), such as seismic lines and small clearings for exploration drill holes.

4.2. Time series analysis of air temperature and global radiation

Air temperature is one of the major factors driving vegetation productivity; therefore the trend and variability in NDVI cannot be explained without considering the influence of this parameter. Temporal trends in air temperature were evaluated for the period from 1977 to 2002 using measurements from five meteorological stations closest to the mining development. Hourly measurements were sequentially averaged over progressively longer periods of time; first over 24 h to obtain average daily temperatures, then daily temperatures were averaged over 10 days to coincide with satellite 10 days composite data, and finally over spring–winter (November–March) and summer–autumn (April–October) to evaluate the multiyear trend.

Fig. 9 presents the time series of average seasonal and yearly air temperatures. The multiyear trend for the most recent 25 years was extracted using the seasonal-trend decomposition procedure. The yearly average temperature graph shows a slight increasing trend from 1997 to 2001. Although, when the same data were separated based on spring–winter and summer–autumn periods, the trend analysis reveals a significant increasing trend in winter–spring temperatures and somewhat less prominent trend for the summer–autumn period. To evaluate if this trend was due to shorter winters or an actual increase in air temperature, the average monthly means were analyzed for the period from 1977 to 2002. A considerable increasing trend was evident only in November and December months (Fig. 10), while the time series for April and May appeared to be stationary (Fig. 11). Therefore, it is concluded that the air temperature time series shows no evidence for an earlier start of the growing season, but offers evidence for warmer winter temperatures (average increase of 5 °C in December and 3 °C in November). The time series of the mean air temperatures in July and August show an increasing trend (1.8 °C) for the same 25-year period (Fig. 12).

Similar trend analysis was performed for global radiation using hourly measurements provided by the

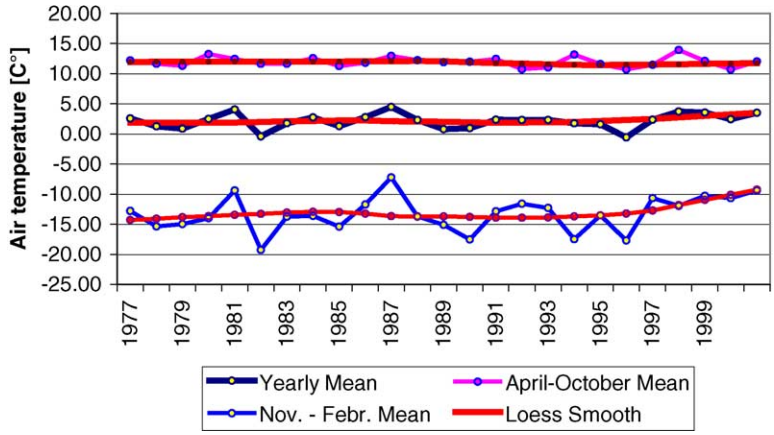

Fig. 9. Time series of the air temperature in Athabasca Oil Sends region 1977–2002. Graph shows yearly and seasonal average temperature during April–October and November–February.

WBEA air-monitoring network. The available time series for the period from 1 January 1998 to 30 August 2002 plotted in Fig. 13 shows the stable seasonal variations with similar annual means. These results suggest that vegetation in the AOS region should exhibit an increasing trend in NPP considering that the average temperature has increased during the analyzed period and is a major driving factor of growth in the boreal ecosystem.

4.3. Cumulative secondary impact assessment

4.3.1. NDVI time series

It is assumed that the pattern of inter-annual NDVI variations should match the pattern of inter-annual variations in growing conditions. Any significant deviations between these two patterns would suggest the influence of other factors on vegetation growth. In the case of AOS region these factors could be related to the mining development. To examine this assumption the NDVI and air temperature time series were prepared with the same 10-day time step and analyzed for periodicity trends (monthly, seasonal, annual), changes in mean (stationarity) and changes in variance (heteroscedasticity).

As for the direct impacts, the analysis was performed for each impact zone separately, but for this analysis the impact zones were defined as potential acid input rings. Anthropogenic classes defined in the 2001-landscape classification were

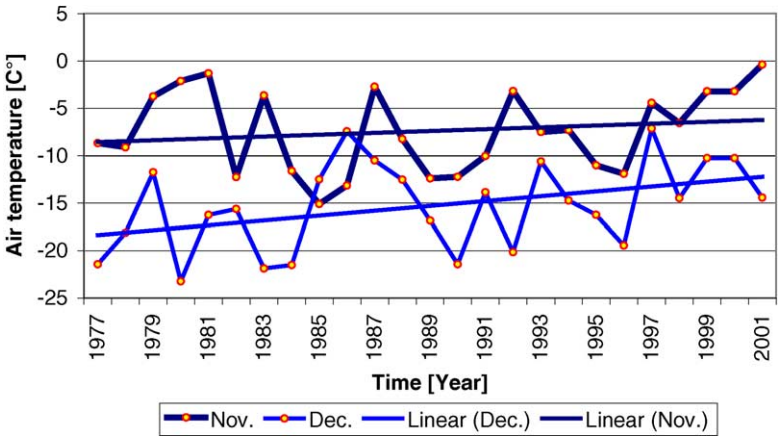

Fig. 10. Time series of air temperature Athabasca Oil Sends region 1977–2002, March and April monthly means.

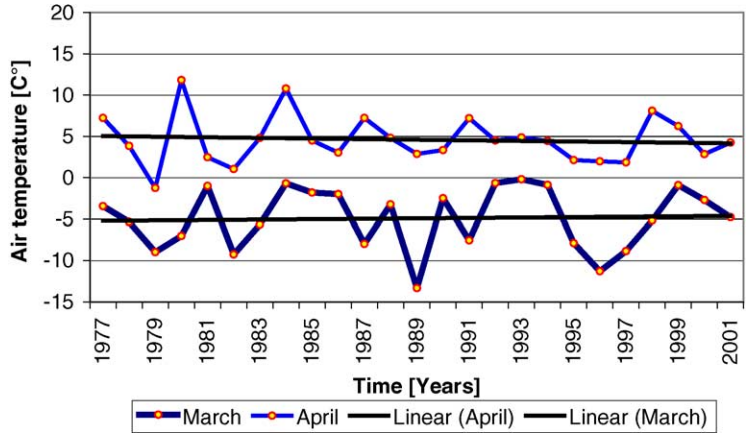

Fig. 11. Time series of air temperature Athabasca Oil Sends region 1977–2002, November–December monthly means.

masked out i.e. only physically undisturbed vegetation present in each ring was included. The areas disturbed by forest fires in last 30 years were also excluded from the analyzed area because intensive post-fire regeneration would cause an increasing trend in NDVI leading to an inappropriate assessment of secondary impacts. The areas affected by fire were identified using forest fire provincial monitoring data.

The NDVI time series were computed from red and near infrared corrected AVHRR and VGT surface reflectance for each 10-day period from April to October (Fig. 14). The same figure also shows trend, cyclical and stochastic components for Ring-PAI 0.25. Each point in the graph represents an average NDVI value computed from 10-day image composites of all pixels located in the area delineated by the PAI isopleths. The NDVI trend was extracted using the STL algorithm.

The trend analysis showed NDVI long-term variations around the mean value with a period of about 6–7 years. A similar long-term pattern is also present in the air temperature variations (Fig. 15). The pattern in the cyclical component follows seasonal variations of green up–peek greenness–senescence,

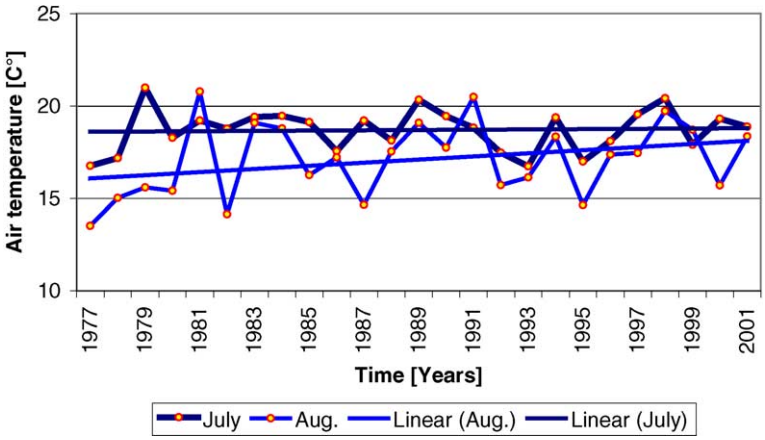

Fig. 12. Time series of air temperature Athabasca Oil Sends region 1977–2002, July–August monthly means.

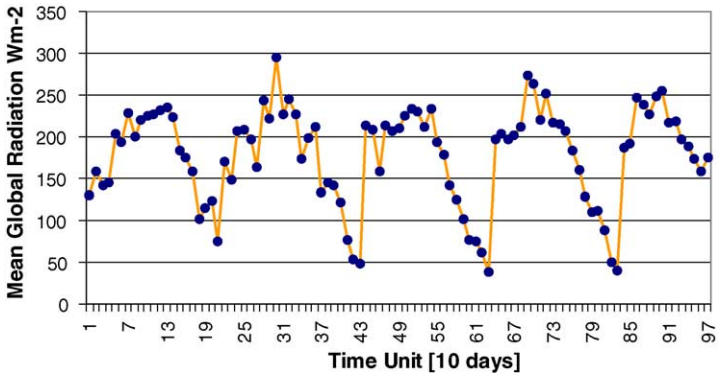

Fig. 13. Time series global radiation Athabasca Oil Sends region 1998–2000, 10-day means.

with a somewhat different phase indicating some variations in the length of growing seasons. The stochastic component exhibits random patterns throughout entire period with average amplitude around mean of about 0.06%.

The comparison of NDVI and air temperature time series (Figs. 14 and 15) confirmed the expected strong correlation. Measurements obtained by AVHRR and VGT for the overlap period 1998–2002 show good agreement. A good general agreement in the long and short-term variations in the patterns of NDVI measured and air temperature over AOS region increases confidence in NDVI as an indicator of vegetation productivity and its sensitivity to local conditions.

4.3.2. KRI ring analysis

To evaluate the pattern in vegetation growth over the entire AOS Region, the KRI was analyzed for each PAI ring during the period from 1990 to 2002. The analysis only included the same physically undisturbed vegetation as in the previous NDVI analysis. The KRI was computed only for June and August to minimize differences due to the longevity of the growing season and noise caused by increased cloud cover during the spring season. The KRI time series normalized to 1990 are illustrated in Fig. 16, all rings show the same general pattern in inter-annual variations. A decrease of 15% for the period 1990–1992 suggesting that the northern biosphere suffered an abrupt decline in vegetation productivity followed

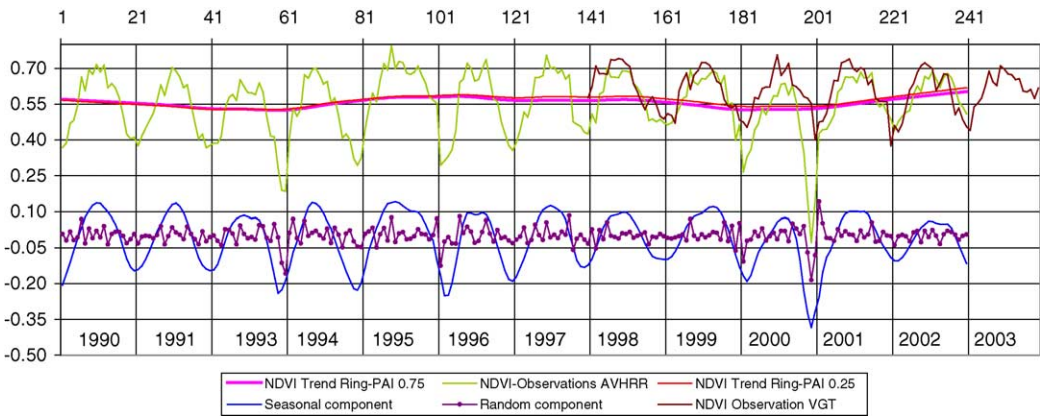

Fig. 14. NDVI time series 1990–2002 derived from 10-days AVHRR composites for impact ring $0.25 > \text{PAI} < 0.50$. Trend, seasonal and random components extracted using seasonal-trend decomposition algorithm.

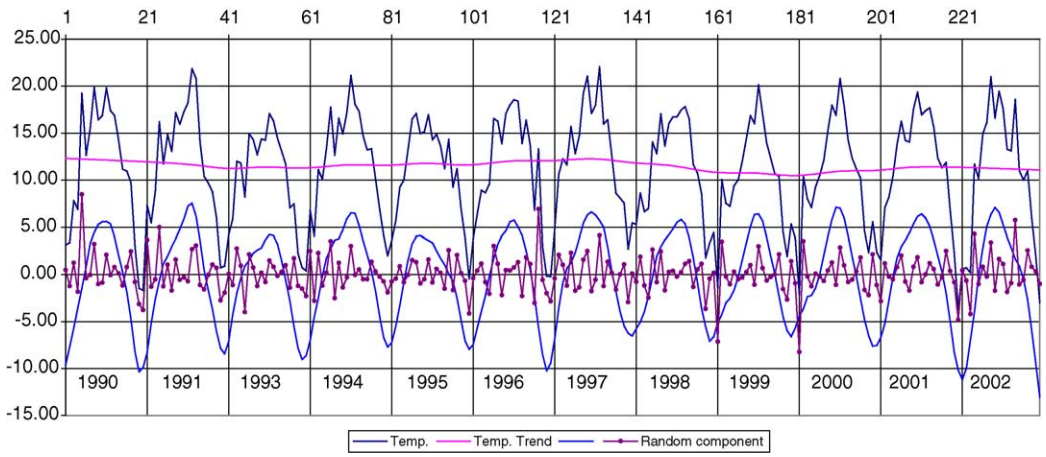

Fig. 15. Ten days average air temperature time series 1990–2002. Trend, seasonal and random components were extracted using seasonal-trend decomposition algorithm.

by an increasing greening trend in 1993. Lucht et al. (2002) also reported the same anomaly in their study of the northern biosphere. They suggested that the anomaly was caused by the Mount Pinatubo volcano eruption in 1991, which expelled dust particles into the atmosphere blocking incoming solar radiation leading to cooler temperatures and a shorter growing season. The ring analysis showed a light decline in vegetation productivity since 1997 for all rings, but more pronounced in the ring closest to the mining development. This declining trend is opposite to the expected trend estimated by the KRI model simulation, which takes into account only climate conditions. It is also opposite to the general finding that there has been a greening trend in the high northern latitudes associated with a slight warming of boreal forest. The observed decline in ring PAI 0.75 in vegetation productivity is still small and within range of natural variations; therefore, it cannot be attributed with high certainty only to the secondary impacts due to emissions from the mining development. It is possible that the ring closest to the mining development contains more small disturbances, for example, seismic lines and roads that were not excluded from

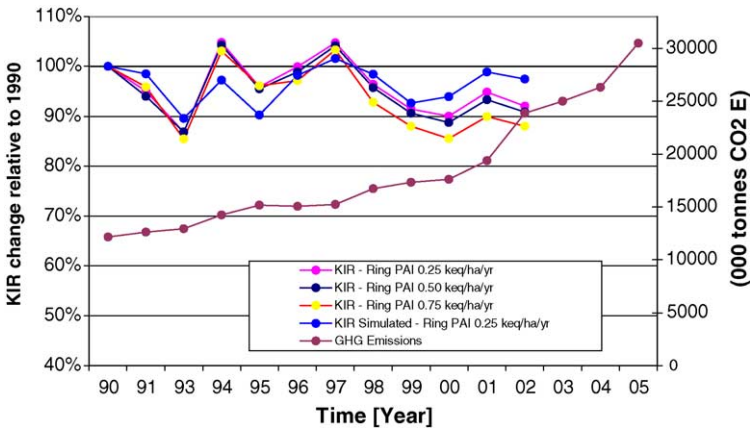

Fig. 16. Surface mining impacts on the surrounding vegetation in function of mine proximity in Athabasca Oil Sends region relative to 1990. Difference in KRI estimated from the remote sensing measurements and KRI predicted by the model simulation are attributed to impact.

the analyzed area due to the coarse spatial resolution (1 km) of satellite data. However, the decreasing trend is evident and proportional to the increase in oil sands production quantified by the amount of CO_2 equivalent emissions (Fig. 16). Continued monitoring in incoming years when mining development is going to be intensified will provide more opportunity to evaluate this remote sensing based initial assessment procedure.

5. Conclusions

A remote sensing based approach for quantifying primary and secondary impacts of surface mining is presented and applied for the assessment of the mining development in Athabasca Oil Sands region. Affected areas were identified as the difference between land cover maps derived from LANDSAT data (30 m resolution) acquired in 1992 and 2001. Maps produced from remote sensing data provide information for subsequent impact assessments from surface mining development on land cover, as well as forming the basis for reclamation planning and monitoring.

A procedure based on AVHRR data with ~1 km spatial resolution provides information on vegetation multi-year condition over large areas for assessing secondary impacts. The analysis of NDVI time series (1990–2002), air temperature and global radiation over the AOS region, shows that inter-annual variations in greenness and growing season length were quantitatively consistent with independent expectations on the basis of climate variability. It was found that air temperature alone accounted for most of the inter-annual variations, but also a slight decrease in vegetation greenness was apparent in close proximity to the mining development.

Understanding the cause of variability in vegetation conditions allows for distinguishing natural from human-induced perturbations of ecosystems; an important pre-requisite in quantifying environmental impacts caused by mining and other developments. However, it is important to point out that the procedure presented here requires a somewhat complicated procedure for correction and normalization of remote sensing data, including across sensor calibration, atmospheric correction, normalization for surface anisotropy-BRDF effects, screening for cloud and other contaminants often present on remote sensing observations. In addition to high quality remote sensing data, a comprehensive knowledge of conditions that a study area was subject to in the past and present is essential for appropriate interpretation leading to higher confidence in obtained results. The same can be concluded for secondary impact assessment: that remote sensing observations are not always sufficient to fully understand cause–effect relationships between industrial development and environmental response, thus they may need to be combined with other field-based measurements.

Acknowledgements

We would like to thank to Bert Guindon from the Canadian Centre of Remote Sensing for his useful input and review during manuscript preparation. We also gratefully acknowledge the support of the Wood Buffalo Environmental Association for providing climate data used in this study.

References

Anderson, A.T., 1977. Landsat imagery for surface mining inventory. Photogrammetric Eng. Remote Sens. 8, 1027–1036.

Barr, D.J., 1981. Landsat application to surface mining. In: Proceedings of the International Conference on Computing in Civil Engineering, New York, May 12–14, American Society of Civil Engineers, Reston, VA, pp. 384–396.

Beaubien, J., 1986. Visual interpretation of vegetation through digitally enhanced Landsat MSS images. Remote Sens. Rev. 2, 11–43.

Benedetti, R., Rossini, P., 1993. On the use of NDVI profiles as a tool for agricultural statistics. The case study of wheat yield estimate and forecast in Emilia Romagna. Remote Sens. Environ. 45, 311–326.

Box, E.O., Holben, N.B., Kalib, V., 1989. Accuracy of the AVHRR vegetation index as a predictor of biomass, primary productivity and net CO_2 flux. Vegetatio 80, 71–89.

Cleveland, B.R., Cleveland, S.W., McRae, J.E., Terpenning, I., 1990. STL: a seasonal-trend decomposition procedure based on loess. J. Off. Stat. 6, 3–73.

Cihlar, J., Latifovic, R., Chen, J.M., Li, Z., 1999. Testing near-real time detection of contaminated pixels in AVHRR composites. Can. J. Remote Sens. 25, 160–170.

Cihlar, J., Hung, L., Xiao, Q., 1996. Land cover classification with AVHRR multichannel composite in northern environments. Remote Sens. Environ. 58, 36–51.

Cihlar, J., Latifovic, R., Chen, J.M., Trishchenko, A.P., Du, Y., Fedosejevs, G., Guindon, B., 2004. Systematic corrections of

AVHRR image composites for temporal studies. Remote Sens. Environ. 89, 217–233.

Cihlar, J., Xiao, Q., Beaubien, J., Fung, K., Latifovic, R., 1998. Classification by progressive generalization: a new automated methodology for remote sensing multichannel data. Int. J. Remote Sens. 19, 2685–2704.

Cramer, W., Kicklighter, W.D., Bondeau, A., Moore, B., Churkina, G., Nemry, B., Ruimy, A., Schloss, A., the Participants of the Potsdam NPP Model Intercomparison, 1999. Comparing global models of terrestrial net primary productivity (NPP): overview and key results. Glob. Change Biol. 5 (Suppl. 1), 1–15.

DeFries, R., Hansen, M., Townshend, J.R.G., 1995. Global discrimination of land cover types from metrics derived from AVHRR Pathfinder Data. Remote Sens. Environ. 54, 209–222.

Du, Y., Cihlar, J., Beaubien, J., Latifovic, R., 2001. Radiometric normalization, compositing and quality control for satellite high resolution image mosaics over large areas. IEEE Trans. Geosci. Remote Sens. 39 (3).

Ducemin, B., Goubier, J., Currier, G., 1999. Monitoring phenological key stages and cycle duration of temperate deciduous forest ecosystems with NOAA/AVHRR data. Remote Sens. Environ. 67, 68–82.

Ecological Stratification Working Group, 1995. A National Ecological Framework for Canada. Agriculture and Agri-Food Canada, Research Branch, Centre for Land and Biological Resources Research and Environment Canada, State of the Environment Directorate, Ecozone Analysis Branch, Ottawa/Hull. Report and National Map at 1:7 500 000 scale.

Environmental Protection Agency, 1995. A User's Guide for the CALPUFF Dispersion Model. EPA-454/B-95-006.

Fedosejevs, G., O'Neill, N.T., Royer, A., Teillet, P.M., Bokoye, A.I., McArthur, B., 2000. Aerosol optical depth for atmospheric correction of AVHRR composite data. Can. J. Remote Sens. 26, 273–284.

Gopal, S., Sklarew, D., Lambion, E., 1994. Fuzzy-neural networks in multi-temporal classification of land-cover change in the Sahal. In: Proceedings of the DOSES.

Goward, S.N., Tucker, J.C., Dye, G.D., 1985. North American vegetation patterns observed with the NOAA-7 advanced very high resolution radiometer. Vegetatio 64, 3–14.

Jang, C.J., Nishigami, Y., Yanagisawa, Y., 1996. Assessment of global forest change between 1986 and using satellite-derived terrestrial net primary productivity. Environ. Conserv. 23, 315–321.

Jarvis, P.G., 1976. The interpretation of the variations in leaf water potential and stomal conductance found in canopies in the field. Philos. Trans. Roy. Soc. Lond. Ser. B: Biol. Sci. 273, 593–610.

Justice, C.O., Townshend, J.R.G., Holban, B.N., Tucker, C.J., 1985. Analysis of the phonology of global vegetation using meteorological satellite data. Int. J. Remote Sens. 6, 1271–1318.

Krupa, S.V., Kickert, R.N., 1989. The greenhouse effect: impacts of ultraviolet-B (UV-B) radiation, carbon dioxide (CO_2) and ozone (O_3) on vegetation. Environ. Pollut. 62, 263–393.

Kumar, M., Monteith, L.J., 1981. Remote Sensing of crop growth. In: Smith, H. (Ed.), Plants and the Daylight Spectrum. Academic Press, San Diego, CA, pp. 133–144.

Latifovic, R., Cihlar, J., Beaubien, J., 1999. Clustering methods for unsupervised classification. In: Proceedings of the 21st Canadian Remote Sensing Symposium, II-509-II-515, Ottawa.

Latifovic, R., Cihlar, J., Chen, J.M., 2001. A comparison of BRDF models for the normalisation of satellite optical data to a standard sun-target-sensor geometry. IEEE Trans. Geosci. Remote Sens. 41 (7).

Loveland, T.R., Merchant, J.W., Ohlen, D.O., Brown, J.F., 1991. Development of a land cover characteristics database for the conterminous U.S.. Photogrammetric Eng. Remote Sens. 57, 1453–1463.

Loveland, T.R., Belward, A.S., 1997. The IGBP-DIS global 1 km land cover data set, DISCover: first result. Int. J. Remote Sens. 18, 3289–3296.

Lucht, W., Colin, C.I., Myneni, B.R., Sitch, S., Friedlingstein, P., Cramer, W., Bousquet, P., Buermann, W., Smith, B., 2002. Climatic control of the high-latitude vegetation greening trend and pinatubo effect. Science 296 .

Malingreau, J.P., 1986. Global vegetation dynamics: satellite observations over Asia. Int. J. Remote Sens. 7, 1121–1146.

Malingreau, J.P., Tucker, C.J., LaPorte, N., 1989. AVHRR for monitoring global tropical deforestation. Int. J. Remote Sens. 10 (4/5), 855–867.

Mamula, N., 1978. Remote sensing methods for monitoring surface coal mining in the Northern Grate Plains. U.S. Geol. Surv. J. Res. 6, 149–160.

Markon, C.J., Peterson, M.K., 2002. The utility of estimating net primary productivity over Alaska using baseline AVHRR data. Int. J. Remote Sens. 23 (21), 4571–4596.

Nenami, R., Running, S., 1997. Landcover characterization using multitemporal red near-IR and thermal IR data from NOAA/AVHRR. Ecol. Approaches 7, 79–90.

Olthof, I., King, D.J., 2000. Development of a forest health index using multispectral airborne digital camera imagery. Can. J. Remote Sens. 26 (3), 166–176.

Prakash, A., Gupta, R.P., 1998. Land-use mapping and change detection in a coal mining area—a case study in the Jharia coalfield, India. Int. J. Remote Sens. 19 (3), 391–410.

Ress, W.G., Williams, M., 1997. Monitoring changes in land cover induced by atmospheric pollution in Kola Peninsula, Russia, using Landsat MSS data. Int. J. Remote Sens. 18 (8), 1703–1723.

Running, W.S., Ramakrishna, N.R., 1988. Relating seasonal patterns of the AVHRR vegetation index to simulated photosynthesis and transpiration of forest in different climates. Remote Sens. Environ. 34 (24), 347–367.

Sallers, J.P., 1985. Canopy reflectance, photosynthesis and transpiration. Int. J. Remote Sens. 6 (8), 1335–1372.

Sallers, J.P., 1987. Canopy reflectance, photosynthesis, and transpiration. II The role of biophysics in the linearity of their interdependence. Remote Sens. Environ. 21, 143–183.

Sallers, J.P., Berry, A.J., Callatz, J.G., Field, B.C., Hall, G.F., 1992. Canopy reflectance, photosynthesis, and transpiration. III A reanalysis using improved leaf models a new canopy integration scheme. Remote Sens. Environ. 42, 187–216.

Schmidt, H., Glaesser, C., 1998. Multitemporal analysis of satellite data their use in the monitoring of the environmental impact of

open cast mining areas in Eastern Germany. Int. J. Remote Sens. 19 (12), 2245–2260.

Schneider, S., 1984. Angewandte Fernerkundung: Methoden und Beispele. Westermann Verlag, Stuttgart.

Stewart, J.B., 1988. Modelling surface conductance of pine forest. Agric. For. Meteorol. 43, 19–35.

Townshend, J.G.R., Justice, C., Li, W., Gurnay, C., Mcmanus, J., 1991. Global land cover classification by remote sensing present capabilities and future possibilities. Remote Sens. Environ. 35, 243–255.

Townshend, J.G.R., 1994. Global data sets for land cover applications from the advanced very high resolution radiometer: an introduction. Int. J. Remote Sens. 15, 3319–3332.

Trishchenko, P.A., Cihlar, J., Li, Z., 2001. Effects of spectral response function on surface reflectance and NDVI measured with moderate resolution satellite sensors. Remote Sens. Environ. 81, 1–18.

Trishchenko, P.A., Hwang, B., Li, Z., 2002. Atmospheric Correction of Satellite Signal in Solar Domain: Impact of Improved Molecular Spectroscopy. Twelfth ARM Science Team Meeting Proceedings, St. Petersburg, Florida.

Tucker, C.J., Townshend, J.R.G., Goff, T.E., 1985. African land cover classification using satellite data. Science 227, 369–375.

Tucker, C.J., Sallers, J.P., 1986. Satellite remote sensing of primary production. Int. J. Remote Sens. 7, 1395–1416.

Wright, P., Stow, R., 1999. Detecting mining subsidence from space. Int. J. Remote Sens. 20 (6), 1183–1188.